THE JOURNAL OF BIOLOGICAL CHEMISTRY VOL. 286, NO. 41, pp. 35966–35976, October 14, 2011

Dynamin Inhibition Blocks Botulinum Neurotoxin Type A Endocytosis in Neurons and Delays Botulism*

Received for publication, July 19, 2011 Published, JBC Papers in Press, August 5, 2011, DOI 10.1074/jbc.M111.283879

Callista B. Harper[‡], Sally Martin[‡1], Tam H. Nguyen[‡1], Shari J. Daniels[‡], Nickolas A. Lavidis[§], Michel R. Popoff[¶], Gordana Hadzic[‖], Anna Mariana[**], Ngoc Chau[**], Adam McCluskey[‖], Phillip J. Robinson[2], and Frederic A. Meunier[‡2,3]**

From the [‡]Queensland Brain Institute, [§]School of Biomedical Sciences, the University of Queensland, Brisbane, Queensland 4072, Australia, the [¶]Unité des Bactéries anaérobies et Toxines, Institut Pasteur, 28 rue du Dr. Roux, 75724 Paris cedex, France, the [‖]Centre for Chemical Biology, Chemistry Building, the University of Newcastle, Callaghan, New South Wales 2308, Australia, and the [**]Children's Medical Research Institute, the University of Sydney, Sydney, New South Wales 2145, Australia

The botulinum neurotoxins (BoNTs) are di-chain bacterial proteins responsible for the paralytic disease botulism. Following binding to the plasma membrane of cholinergic motor nerve terminals, BoNTs are internalized into an endocytic compartment. Although several endocytic pathways have been characterized in neurons, the molecular mechanism underpinning the uptake of BoNTs at the presynaptic nerve terminal is still unclear. Here, a recombinant BoNT/A heavy chain binding domain (Hc) was used to unravel the internalization pathway by fluorescence and electron microscopy. BoNT/A-Hc initially enters cultured hippocampal neurons in an activity-dependent manner into synaptic vesicles and clathrin-coated vesicles before also entering endosomal structures and multivesicular bodies. We found that inhibiting dynamin with the novel potent Dynasore analog, Dyngo-4a™, was sufficient to abolish BoNT/A-Hc internalization and BoNT/A-induced SNAP25 cleavage in hippocampal neurons. Dyngo-4a also interfered with BoNT/A-Hc internalization into motor nerve terminals. Furthermore, Dyngo-4a afforded protection against BoNT/A-induced paralysis at the rat hemidiaphragm. A significant delay of >30% in the onset of botulism was observed in mice injected with Dyngo-4a. Dynamin inhibition therefore provides a therapeutic avenue for the treatment of botulism and other diseases caused by pathogens sharing dynamin-dependent uptake mechanisms.

Among neurotoxins acting presynaptically (1–3), botulinum neurotoxins (BoNTs)[4] comprise a group of highly lethal toxins consisting of seven serotypes (BoNT/A–G) produced by the anerobic bacteria, *Clostridium botulinum*. Due to the extreme potency of BoNTs and the relative ease with which the pathogens can be cultured, these neurotoxins are well known biological weapons (4, 5). This has prompted a number of investigations into the discovery of drugs that could prevent or treat botulism (6, 7). Currently, the only available therapy is restricted to vaccines and antitoxins (7). However, vaccination precludes the use of BoNTs as a therapeutic, and treatments based on antitoxins are difficult to implement because of limited supply and the short time window available for administration (5). Alternative drugs are therefore needed, with most work focusing on inhibitors of the light chain (Lc) proteolytic activity (8).

BoNTs target cholinergic motor nerve terminals, promoting a block in acetylcholine release, which results in a flaccid paralysis known as botulism (6, 9, 10). They are di-chain bacterial toxins, comprising a 100-kDa heavy chain connected by a disulfide bond to a 50-kDa Lc. The heavy chain is divided into two functionally distinct regions: a binding (Hc) and a translocation (H_N) domain (11). The binding domain initially interacts with low affinity to a group of gangliosides on the presynaptic plasma membrane (12), after which it binds to a protein acceptor (13–18). The neurotoxin is subsequently internalized into an acidic compartment, prompting the translocation domain to create a pore and promoting the release of the Lc into the cytosol following hydrolysis of the disulfide bond (19). The Lc is a zinc metalloprotease that, depending on the serotype, cleaves specific amino acid bonds from SNARE proteins (20–25), resulting in a blockade of neurotransmission and flaccid paralysis (9, 26).

Although BoNT/A is believed to enter neurons through the endocytosis of synaptic vesicles (17, 27), the actual mechanism underpinning its uptake remains ill defined. BoNT/A has recently been shown to enter an early endosomal compartment in a neuroblastoma cell line (28), suggesting that this trafficking pathway could also contribute to its pathogenicity. In view of the role played by dynamin-mediated fission of endocytic vesicles from the plasma membrane (29), we hypothesized that dynamin might play an important role in initiating the neuronal uptake of BoNT/A.

In this paper, we show that Dyngo-4a™ (30), a novel, highly potent dynamin inhibitor, prevents the uptake of BoNT/A-Hc in cultured hippocampal neurons and in motor nerve terminals. We also demonstrate that Dyngo-4a treatment inhibits BoNT/A-induced paralysis at the rat hemidiaphragm and sig-

* This work was supported by the Australian National Health and Medical Research Council. Dyngo-4a™ and Dyngo™ are trademarks of the authors' institutions and affiliates, the Children's Medical Research Institute and Newcastle Innovation, Ltd. (the commercial arm of the University of Newcastle), which have entered into a commercial license agreement with Ascent Scientific, Ltd. (Bristol, United Kingdom) to market and distribute Dyngo-4a as a research tool globally.

[1] Both authors contributed equally to this work.

[2] National Health and Medical Research Council Research Fellows.

[3] To whom correspondence should be addressed. Tel.: 61-7-3346-66373; Fax: 61-7-3346-6301; E-mail: f.meunier@uq.edu.au.

[4] The abbreviations used are: BoNT, botulinum neurotoxin; DMSO, dimethyl sulfoxide; Hc, heavy chain; Lc, light chain; MVB, multivesicular body; NMP, 1-methyl-2-pyrrolidione; VAMP2, vesicular associated membrane protein-2.

nificantly delays the onset of botulism in mice. Dynamin is therefore a potential therapeutic target for counteracting botulism.

EXPERIMENTAL PROCEDURES

Protein Expression—The His_6-tagged BoNT/A-Hc was purified using Co IDA-agarose (Scientifix) as described previously (28) and conjugated to Alexa Fluor 488 C_5 maleimide (Invitrogen) according to the manufacturer's instructions.

Antibodies—His_6 (Cell Signaling Technology), β-actin (Abcam), vesicular associated membrane protein-2 (VAMP2) 69.1 (Synaptic Systems, Goettingen), βIII-tubulin (Covance), Rab5 (Cell Signaling Technology), and BoNT/A-truncated SNAP25 (kind gift from D. Sesardic) were used.

Dynamin Inhibitor—Dyngo-4a is available from Ascent Scientific Ltd. (Bristol). Dyngo-4a was made up in DMSO (30 mM) for *in vitro* experiments and dissolved in a formulation containing 1-methyl-2-pyrrolidione (NMP) and polyethylene glycol 300 (PEG300) (1 part NMP to 9 parts PEG300), then diluted 1/9 in phosphate-buffered saline (PBS) for *in vivo* experiments. GTPase assays and IC_{50} determination for inhibition of lipid-stimulated dynamin activity were performed as described previously for endogenous sheep brain dynamin I and insect cell (Sf21)-expressed rat dynamin II, except that the GTPase assay buffer contained 5 mM Tris-HCl, 10 mM NaCl, 2 mM Mg^{2+}, pH 7.4, 1 μg/ml leupeptin, 0.1 mM PMSF and 0.3 mM GTP (31).

Internalization Studies—Cultured hippocampal neurons were prepared from embryonic age 18 C57BL/6 embryos and co-cultured with astroglia as described previously (32). The neurons were allowed to mature for at least 14 days *in vitro* before use. Neurons were removed from the co-culture and incubated for 5 min at 37 °C with 100 nM Alexa Fluor 488-BoNT/A-Hc in a low K^+ buffer (15 mM HEPES, 145 mM NaCl, 5.6 mM KCl, 2.2 mM $CaCl_2$, 0.5 mM $MgCl_2$, 5.6 mM D-glucose, 0.5 mM ascorbic acid, 0.1% bovine serum albumin (BSA), pH 7.4) or high K^+ buffer (modified to contain 95 mM NaCl and 56 mM KCl) (18), with or without Dyngo-4a or Dynasore as indicated. The cells were fixed with 4% paraformaldehyde, processed for immunocytochemistry (33), imaged (LSM510 confocal microscope; Zeiss), and analyzed using Zen software (Zeiss) or LaserPix (Bio-Rad).

Electron Microscopy—Colloidal gold (5.5 nm) was prepared as described previously (34), conjugated to BoNT/A-Hc, and stabilized with 0.1% BSA. Monodispersed BoNT/A-Hc-gold was washed and concentrated by centrifugation (35) and stored in PBS at 4 °C. Primary hippocampal neurons (15 days *in vitro*) were incubated with a 1/10 dilution of BoNT/A-Hc-gold as described in the internalization studies. Cells were subsequently washed in PBS and fixed with 2.5% glutaraldehyde in PBS. Fixed cells were contrasted with 1% osmium tetroxide and 4% uranyl acetate prior to dehydration and embedding in LX-112 resin. Sections (~50 nm) were cut using an ultramicrotome (UC64; Leica). BoNT/A-Hc-gold endocytosis was quantified by systematic random sampling using a transmission electron microscope (model 1011; JEOL) equipped with a Morada cooled CCD camera. Neurites were visualized at 60,000 ×, and the number of gold particles contained within endocytic structures was recorded. A 200 nm square lattice grid was overlaid on the same sections using the iTEM AnalySIS software, and grid intersections falling on neurites or presynaptic areas were also recorded.

BoNT/A-Hc Internalization at the Amphibian Neuromuscular Junction—The iliofibularis muscles of adult toads (*Bufo marinus*) were prepared as described previously (36). BoNT/A-Hc internalization was carried out in high K^+ frog Ringer's solution (62 mM NaCl, 56 mM KCl, 1.8 mM $CaCl_2$, 1 mM $MgCl_2$, 5 mM HEPES-OH, pH 7.4). Control and Dyngo-4a-treated (30 μM, 40 min) preparations were chilled on ice for 5 min prior to the addition of 800 nM Alexa Fluor 488-BoNT/A-Hc and 1 μM Alexa Fluor 555-α-bungarotoxin (Invitrogen) for 20 min on ice. They were then washed with normal frog Ringer's solution (116 mM NaCl, 2 mM KCl, 1.8 mM $CaCl_2$, 1 mM $MgCl_2$, 5 mM HEPES-OH, pH 7.4) at room temperature and imaged by confocal microscopy (LSM510). Fluorescence recovery after photobleaching experiments were performed by exposing defined regions of cells to 100% argon (488 nm) laser intensity for 20 iterations. Fluorescence intensity was measured in the photobleached area and background using Zeiss LSM510 software. Background was subtracted from each data point. To determine the recovery we normalized values to the intensity prior to bleaching. The mobile fraction was determined by dividing the photobleached region at maximal recovery by the initial photobleached intensity. The halftime was determined by fitting the recovery curve.

SNAP25 Cleavage Assay—Cultured hippocampal neurons were removed from co-culture and washed once with low K^+ buffer. They were then treated with either DMSO or Dyngo-4a (30 μM) for 20 min. Neurons were stimulated with high K^+ buffer with and without BoNT/A (100 pM) in the continuing presence of DMSO or Dyngo-4a for 5 min. The cells were washed five times with low K^+ buffer containing DMSO or Dyngo-4a and left for 90 min before being transferred back to co-culture with astroglia and conditioned medium for a further 24 h. The neurons were then removed from co-culture and processed for Western blotting as follows: the cells were washed twice with ice-cold PBS before scraping in 20 mM HEPES, 150 mM NaCl, pH 7.5, containing protease inhibitors. The cell membranes were collected and resuspended in Laemmli sample buffer containing 10% β-mercaptoethanol. Samples were run on an SDS-PAGE and then transferred to a PVDF membrane. The membrane was probed for cleaved SNAP25 using an antibody designed against the SNAP25-cleaved product, which does not recognize full-length SNAP25 (37, 38). The intensity of the bands was normalized to β-actin, and the integrated intensity was used to determine the amount of cleavage relative to the control (ImageJ).

Rat Phrenic Nerve-Hemidiaphragm Twitch Experiments—The hemidiaphragm and innervating phrenic nerve were dissected from 5-week-old male Wistar rats. The nerve muscle preparation was suspended in an organ bath containing carbogen-bubbled Tyrode's solution (136.7 mM NaCl, 2.68 mM KCl, 1.75 mM NaH_2PO_4, 16.3 mM $NaHCO_3$, 1 mM $MgCl_2$, 1 mM $CaCl_2$, 7.8 mM D-glucose). The nerve was stimulated with 0.1-ms square pulses of 10 V at 0.2 Hz and the force of contractions (mN) was recorded through Powerlab and Bridge Amp Systems (AD Instruments, New South Wales) with Chart soft-

ware (AD Instruments). Upon reaching stable contractions, 30 μM Dyngo-4a or vehicle was added for 1 h prior to the addition of BoNT/A (100 pM). Control preparations were as indicated. Contractions were recorded over 6–8 h and analyzed by converting contractile strength to percentage decline.

In Vivo Assay—BoNT/A was diluted in 0.9% saline containing 0.1 mg/ml BSA, immediately prior to use. Female CD-1 mice (30–40 g) were injected intraperitoneally with 1 mg of Dyngo-4a (which is 30 mg/kg body weight) or vehicle (1/9 NMP/PEG300 (1 part NMP to 9 parts PEG300) in PBS). 1.5–2 h later, mice were injected with $2LD_{50}$ BoNT/A via the tail vein. A top-up of 1 mg of Dyngo-4a or vehicle was administered 4.5–8 h after the initial intraperitoneal injection. Mice were constantly monitored for signs of botulism and euthanized upon development of acute respiratory distress.

RESULTS

Activity-dependent Uptake and Traffic of BoNT/A-Hc in Hippocampal Neurons—His-tagged BoNT/A-Hc was expressed and purified on a Co^{2+}-IDA agarose column, eluted and fluorescently tagged using Alexa Fluor 488 C_5 maleimide (Alexa Fluor 488-BoNT/A-Hc). Western blotting with a His_6 antibody was used to confirm the presence of the protein in the eluate (Fig. 1*A*). Successful conjugation of BoNT/A-Hc to Alexa Fluor 488 was checked by UV illumination of the Western blot membrane (Fig. 1*A*) (28).

BoNTs have previously been reported to enter hippocampal neurons in an activity-dependent manner (17, 18). To validate our probe, hippocampal neurons were incubated with Alexa Fluor 488-BoNT/A-Hc in low or depolarizing high K^+ buffer, then fixed and processed for immunocytochemistry. As expected, in the absence of stimulation there was only a low level of Alexa Fluor 488-BoNT/A-Hc internalization (Fig. 1*B*). In response to depolarization, the uptake of Alexa Fluor 488-BoNT/A-Hc was significantly increased (Fig. 1, *B* and *C*). Importantly, Alexa Fluor 488-BoNT/A-Hc staining partially co-localized with that of VAMP2, suggesting that the uptake was into synaptic vesicles. As expected, the overall intensity level of VAMP2 immunoreactivity was unaffected by stimulation (Fig. 1*D*).

In view of the recent finding that BoNT/A-Hc cellular entry involves early endosomes in neuroblastoma cells (28), we carried out triple labeling to determine the level of co-localization among Alexa Fluor 488-BoNT/A-Hc, VAMP2, and Rab5 (an early endosomal marker). Five-minute depolarization led to 59% of Alexa Fluor 488-BoNT/A-Hc positive vesicles co-localizing with VAMP2-positive puncta (Fig. 2), in agreement with the results of previous studies (17, 18). Interestingly, 34% of Alexa Fluor 488-BoNT/A-Hc/VAMP2 dual-positive compartments also partially or fully co-localized with Rab5-positive compartments, suggesting that Alexa Fluor 488-BoNT/A-Hc can at least partially traffic through synaptic vesicles and early endosomes in hippocampal neurons (Fig. 2). This supports the idea that Rab5 is present on synaptic vesicles, as demonstrated previously (39–42). We observed very few Alexa Fluor 488-BoNT/A-Hc carriers that were Rab5-positive and VAMP2-negative. Furthermore, there were no significant changes at the later chase time points of 30 and 60 min following a 5-min stimulation, although there was a trend toward increased co-localization of Alexa Fluor 488-BoNT/A-Hc with VAMP2, perhaps revealing a limited maturation process (Fig. 2*B*). These results suggest that BoNT/A-Hc enters neurons via activity-dependent synaptic vesicle endocytosis and that it rapidly enters an early endosomal compartment.

To analyze the precise endocytic route, we used electron microscopy of BoNT/A-Hc conjugated to colloidal gold. In resting hippocampal neurons, BoNT/A-Hc clearly bound to the membrane of nerve terminals (Fig. 3*A*). Upon depolarization, BoNT/A-Hc accumulated in endocytic structures of the presynaptic region (Fig. 3, *B–H*). Quantitation demonstrated that the presynaptic area corresponded to 25.2 ± 4.7% of the total neurite area analyzed. Following 5 min of stimulation with high K^+, the nerve terminals contained 73.3 ± 7.1% of the endocytosed BoNT/A-Hc (mean ± S.E., $n = 3$ independent experiments, 11–18 fields analyzed per experiment). BoNT/A-Hc was largely detected in synaptic vesicles but also in clathrin-coated pits and vesicles and in noncoated, electrolucent structures classified morphologically as early endosomal compartments (Fig. 3, *B–F*, and Table 1). A similar distribution of BoNT/A-Hc was observed at the later time point of 30 min, which represented a 5-min stimulation followed by a 25-min chase period (Fig. 3, *G–H*). However, BoNT/A-Hc was also (~10% total) detected in multivesicular bodies (MVBs), both in the region of the synapse and in more distal areas (Fig. 3, *I–K*). The average concentration of BoNT/A-Hc in MVBs was 11.8 ± 2.4 gold particles, with 69.4 ± 6.4% of these labeling the outer face of the intraluminal vesicles ($n = 23$ individual MVBs ± S.E., pooled from two individual experiments). This localization is consistent with BoNT/A-Hc endocytosis into early endosomes and subsequent partitioning into invaginating luminal vesicles during maturation into MVBs (43). Our results therefore support the notion that BoNT/A-Hc enters neurons via synaptic vesicles and further suggest a parallel, slower endocytic route via a clathrin-mediated process and the early endosomal system leading to MVBs.

Dynamin Inhibition Blocks BoNT/A-Hc Internalization—In view of the recently proposed role of dynamin in the uptake of various di-chain bacterial toxins (28, 44–46), we investigated the effect of a novel dynamin inhibitor, Dyngo-4a (30), on the internalization of Alexa Fluor 488-BoNT/A-Hc. Dyngo-4a is a close structural analog of Dynasore, but with an increased potency in cells and *in vitro*. It has an IC_{50} for dynamin I of 380 ± 0.05 nM ($n = 5$ independent experiments), and for dynamin II the IC_{50} is 2.6 ± 0.12 μM ($n = 3$). Hippocampal neurons were depolarized in the presence of Dyngo-4a 20 min prior to the addition of Alexa Fluor 488-BoNT/A-Hc and for a further 5 min in the continuous presence of Dyngo-4a before being washed, fixed, and processed for immunocytochemistry. Dyngo-4a dose-dependently inhibited internalization of Alexa Fluor 488-BoNT/A-Hc at low micromolar concentrations (Fig. 4) with an IC_{50} of 16.0 ± 1.2 μM. The role of dynamin was confirmed by treating hippocampal neurons with Dynasore, which has an IC_{50} for inhibition of dynamin *in vitro* of ~15 μM (47), and inhibited internalization of Alexa Fluor 488-BoNT/A-Hc with an IC_{50} of 79.3 ± 1.3 μM (Fig. 4). Given that BoNTs primarily target cholinergic motor nerve terminals (9), we also tested the ability of Dyngo-4a to prevent Alexa Fluor 488-BoNT/A-Hc internalization at the presynaptic motor nerve ter-

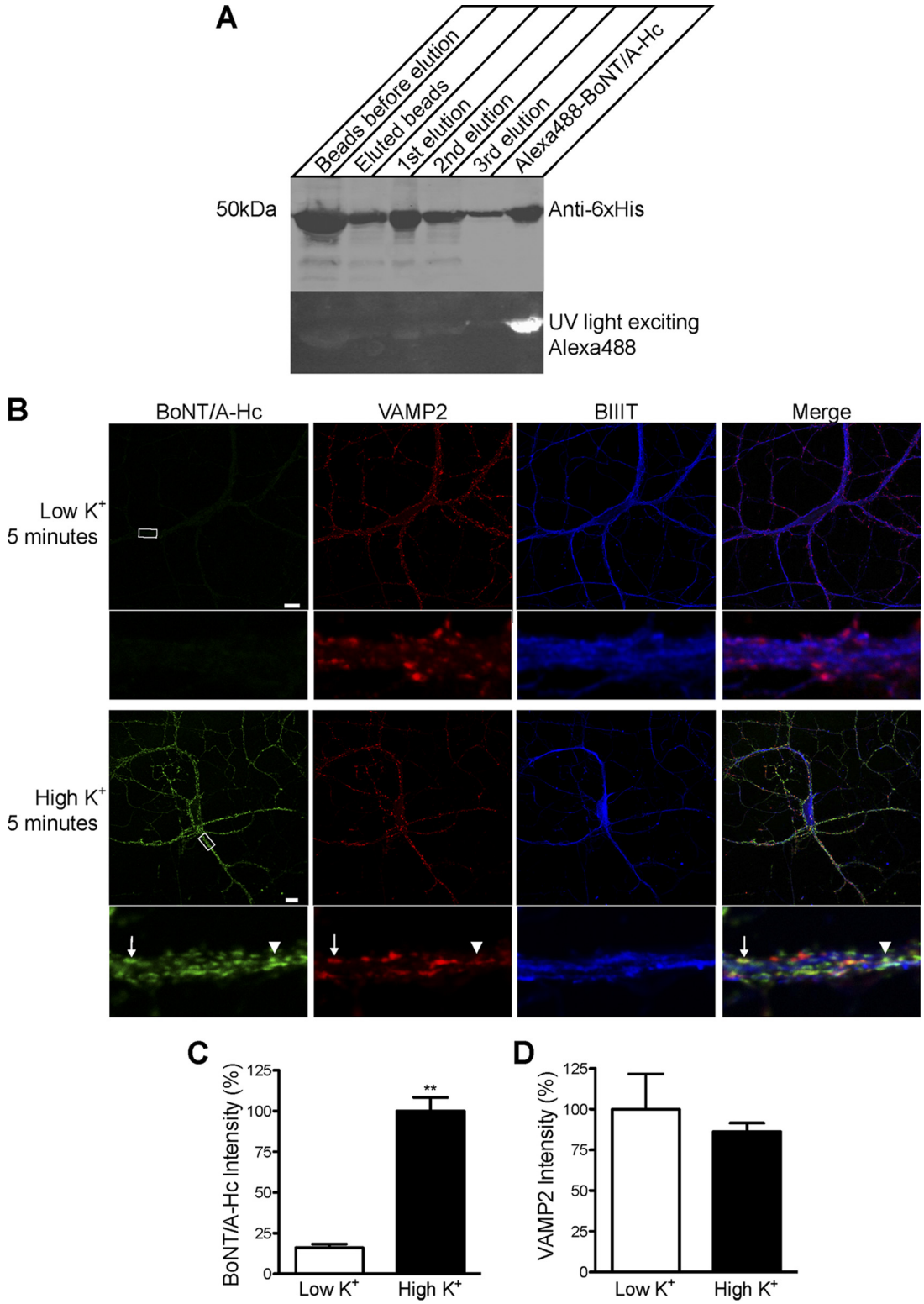

FIGURE 1. **The uptake of Alexa Fluor 488-BoNT/A-Hc in cultured hippocampal neurons is activity-dependent.** *A*, Western blot of BoNT/A-Hc. Recombinant BoNT/A-Hc was expressed and purified on Co^{2+}-IDA agarose before conjugation to Alexa Fluor 488 C_5 maleimide. The fractions (of equivalent volume, 6 μl) indicated on the figure were run on an SDS-PAGE, and Western blotting using a His_6 antibody was carried out to confirm the presence of the protein. The PVDF membrane was exposed to UV light to check the conjugation of the protein. *B*, cultured hippocampal neurons incubated for 5 min with Alexa Fluor 488-BoNT/A-Hc (100 nM) in the absence or presence of high K^+. Neurons were then fixed and processed for βIII-tubulin (*BIIIT*) and VAMP2 immunolabeling. A representative confocal micrograph shows a clear lack of Alexa Fluor 488-BoNT/A-Hc uptake in the absence of high K^+. Uptake of Alexa Fluor 488-BoNT/A-Hc is increased significantly in the presence of high K^+ and shows a partial co-localization with VAMP2 (*arrow*). The *arrowhead* indicates an Alexa Fluor 488-BoNT/A-Hc-positive compartment that does not co-localize with VAMP2. *Scale bars*, 10 μm. *C*, level of Alexa Fluor 488-BoNT/A-Hc uptake in neuritic processes determined as described under "Experimental Procedures." A *t* test revealed a significant increase (**, $p < 0.01$) in fluorescence intensity upon stimulation with high K^+ ($n = 30–38$ regions of interest), two independent experiments). *D*, intensity of VAMP2 immunostaining determined as an internal control to ensure there was no change between tested samples ($n = 30–38$, two independent experiments).

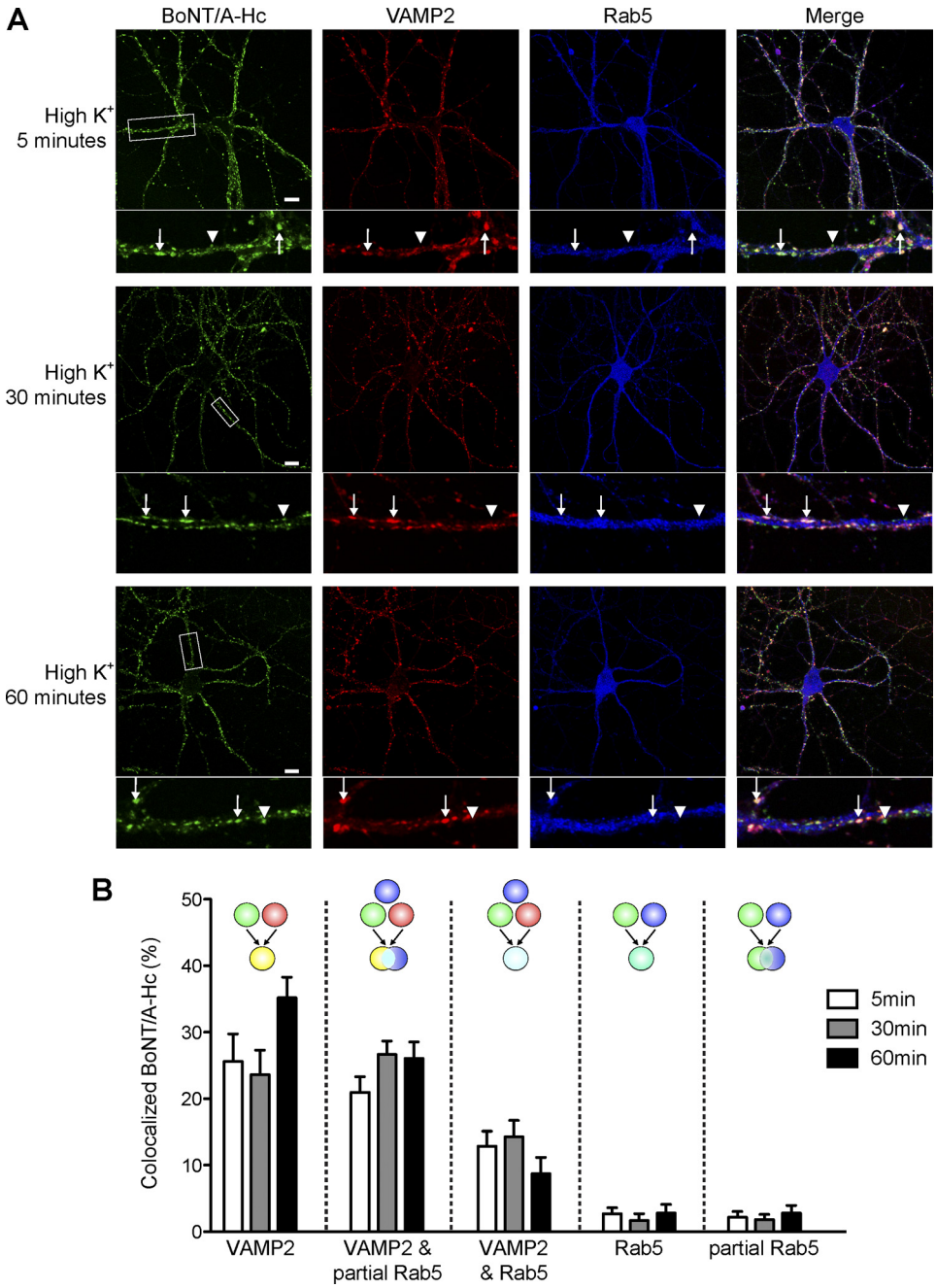

FIGURE 2. **Internalized Alexa Fluor 488-BoNT/A-Hc shows partial co-localization with Rab5 and VAMP2.** Cultured hippocampal neurons were incubated for 5 min in the presence of high K^+ with Alexa Fluor 488-BoNT/A-Hc (100 nM), after which they were washed and incubated in low K^+ buffer for a further 25 or 55 min. The cells were then fixed and processed for immunocytochemistry using VAMP2 and Rab5 antibodies. *A*, representative confocal micrographs show a good degree of co-localization between Alexa Fluor 488-BoNT/A-Hc and VAMP2. In several instances, these compartments showed at least partial co-localization with Rab5 staining (*arrows*). Few Alexa Fluor 488-BoNT/A-Hc-positive structures did not co-localize with either Rab5 or VAMP2 (*arrowheads*). *Scale bars*, 10 μm. *B*, the level of co-localization was quantified by determining the number of Alexa Fluor 488-BoNT/A-Hc-positive compartments that showed co-localization in selected regions of interest in neurites. Alexa Fluor 488-BoNT/A-Hc co-localized mainly with VAMP2. Some of these Alexa Fluor 488-BoNT/A-Hc/VAMP2-positive compartments also showed an either full or partial co-localization with Rab5. Alexa Fluor 488-BoNT/A-Hc rarely co-localized with Rab5 alone (n = 12–17, two or three independent experiments).

minal. Toad iliofibularis neuromuscular junction preparations were isolated and incubated in the presence or absence of Dyngo-4a for 40 min prior to the addition of Alexa Fluor 488-BoNT/A-Hc and α-bungarotoxin. Labeled preparations were then washed extensively prior to confocal imaging of the live neuromuscular junction. Untreated nerve terminals exhibited distinct Alexa Fluor 488-BoNT/A-Hc presynaptic labeling, overlapping with α-bungarotoxin staining (Fig. 5*A*). Unexpectedly, Dyngo-4a-treated neuromuscular junctions also showed Alexa Fluor 488-BoNT/A-Hc staining, but the distribution appeared altered (Fig. 5*A*). Based on these findings, we hypothesized that the staining found in Dyngo-4a-treated preparations mostly reflected Alexa Fluor 488-BoNT/A-Hc binding to the presynaptic plasma membrane, as opposed to the probe being internalized in untreated nerve terminals. To test this possibility, we performed fluorescence recovery after photo-

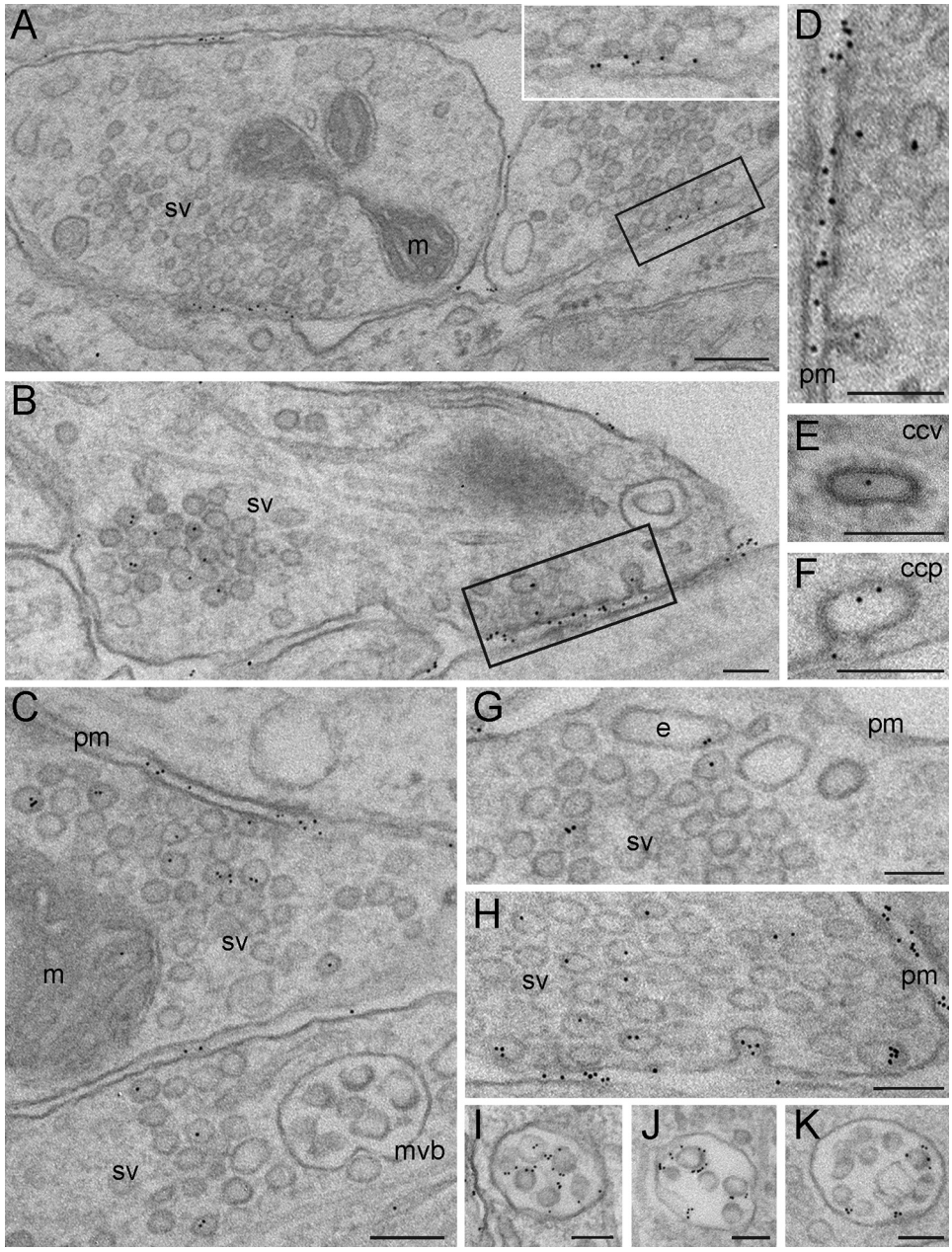

FIGURE 3. **BoNT/A-Hc endocytosis into synaptic vesicles, clathrin-coated vesicles, endosomes, and MVBs.** Hippocampal neurons were incubated with BoNT/A-Hc-gold, after which they were fixed and processed for electron microscopy. The distribution of BoNT/A-Hc-gold in cultured hippocampal neurons was analyzed in unstimulated cells (*A* and *inset*), following a 5-min stimulation (*B–E*), or following a 5-min stimulation and a 25-min chase period (*F–K*). Note that *D* is an enlargement of the *boxed area* in *B*. *m*, mitochondria; *sv*, synaptic vesicles; *pm*, plasma membrane; *e*, endosomes; *ccv*, clathrin-coated vesicles; *ccp*, clathrin-coated pit; *mvb*, multivesicular body. *Scale bars*, 200 nm (*A*) and 100 nm (*B–K*).

TABLE 1

Endocytosed BoNT/A-Hc-gold detected in synaptic vesicles and endocytic compartments

The distribution of internalized BoNT/A-Hc-gold in presynaptic organelles following 5-min stimulation with high K^+ was quantified. Note the clear accumulation of BoNT/A-Hc in synaptic vesicles, with the remaining distributed between clathrin-coated vesicles and endosomes (mean ± S.D., three independent experiments, 11–18 fields each, between 58 and 126 gold particles counted/experiment). In addition, the average number of BoNT/A-Hc-gold particles/vesicle was calculated (mean ± S.D., three independent experiments).

Organelle	Total gold	Gold particles/vesicle
	%	
Synaptic vesicle	78.7 ± 6.6	1.3 ± 0.1
Clathrin-coated vesicle	16.0 ± 6.1	2.2 ± 0.2
Endosome	5.3 ± 7.6	0.9 ± 0.8

bleaching analysis on live neuromuscular junctions with the view that the recovery profile of internalized Alexa Fluor 488-BoNT/A-Hc should be slower than that of plasma membrane-bound probe. The changes in intensity are shown in the kymographs in Fig. 5*B*, with the quantitative analysis of the recovery of fluorescence demonstrating that the recovery of Dyngo-4a-treated nerve terminals was significantly higher than that of untreated preparations (Fig. 5*C*). The mobile fraction of the untreated nerve terminals was 0.083 ± 0.004 whereas that of the Dyngo-4a-treated nerve terminals was 0.510 ± 0.005 ($p < 0.0001$). Similarly, the half-time fluorescence recovery was reduced from 4.57 s to 2.86 s by Dyngo-4a treatment. These

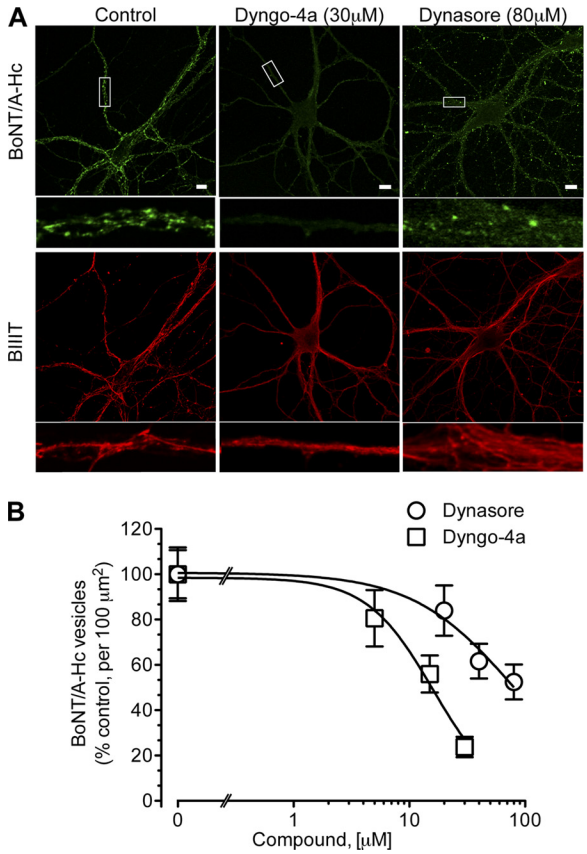

FIGURE 4. **Dynamin inhibition blocks Alexa Fluor 488-BoNT/A-Hc uptake in cultured hippocampal neurons.** *A*, cultured hippocampal neurons were pretreated with increasing concentrations of Dyngo-4a or Dynasore in high K^+ buffer for 20 min before the addition of Alexa Fluor 488-BoNT/A-Hc (100 nM) for a further 5 min. Cells were then fixed and processed for immunocytochemistry with βIII-tubulin (*BIIIT*) antibody, which was used to confirm the neuronal nature of the cells. A representative confocal micrograph shows that treatment with both Dyngo-4a and Dynasore, at the indicated concentrations, substantially reduced the uptake of Alexa Fluor 488-BoNT/A-Hc. *Scale bars*, 10 μm. *B*, the inhibition of Alexa Fluor 488-BoNT/A-Hc by the two inhibitors was quantified by determining the number of Alexa Fluor 488-BoNT/A-Hc-positive vesicles/100 μm^2 in the region of interest in the cell body and neurites. The data were transformed to $x = \log(x)$ and fitted to a nonlinear curve to determine the IC_{50} (16.0 ± 1.2 μM for Dyngo-4a and 79.3 ± 1.3 μM for Dynasore). A one-way ANOVA with Bonferroni's post test confirmed that treatment with 15 and 30 μM Dyngo-4a or 40 and 80 μM Dynasore significantly reduced the uptake of Alexa Fluor 488-BoNT/A-Hc (**, $p < 0.01$, n = 45–60, two or three independent experiments).

experiments demonstrate that Dyngo-4a blocks Alexa Fluor 488-BoNT/A-Hc internalization in motor nerve terminals as well as cultured hippocampal neurons.

Dyngo-4a Prevents BoNT/A-induced SNAP25 Cleavage in Cultured Hippocampal Neurons—BoNT/A promotes paralysis through the cleavage of 9 amino acid residues from the C terminus of SNAP25 (21, 13–25). We next investigated whether Dyngo-4a could prevent the cleavage of SNAP25 in hippocampal neurons. Using an antibody specifically designed to recognize BoNT/A-cleaved SNAP25 (37, 38), hippocampal neurons incubated with BoNT/A alone exhibited a distinct band at ~25 kDa (Fig. 6*A*). However, SNAP25 cleavage could not be detected in the lysate from either control neurons or those treated with Dyngo-4a prior to the addition of BoNT/A (Fig. 6). These results show that Dyngo-4a not only blocks the uptake of the BoNT/A binding domain, but can also prevent intoxication by the active form.

Dyngo-4a Disrupts BoNT/A-induced Paralysis and Delays the Onset of Botulism—Our next goal was to determine whether Dyngo-4a could be used to prevent the muscle paralysis induced by purified BoNT/A. We investigated this using a rat hemidiaphragm twitch model. The muscles were stimulated at 0.2 Hz, and the contractile force was recorded over 6–8 h. Representative traces of the twitch recordings for each condition are shown in Fig. 7*A*. Neither the untreated nor the Dyngo-4a-treated control muscles showed any sign of decline in contractions for up to 8 h. Following addition of BoNT/A, the amplitude of contractions decreased, consistent with BoNT-induced paralysis (48). Muscles pretreated with Dyngo-4a prior to addition of BoNT/A showed significantly less decline in contractile strength (Fig. 7*A* and Table 2). The contractile force, graphed as percent decline in contractions, fitted well to a four-parameter logistic curve ($R^2 = 0.999$ and 0.994) (Table 2). Both the $t_{1/2}$ and the Hill slope were significantly different ($p = 0.0007$ and 0.0018, respectively). These results show that both the decline in contraction and the time to reach 50% of decline were significantly increased in the Dyngo-4a-treated muscles compared with the BoNT/A control group. Together, these results demonstrate that Dyngo-4a provides significant protection against BoNT/A-induced muscle paralysis.

Finally, we asked whether Dyngo-4a could prevent the onset of botulism in an *in vivo* murine model. CD-1 mice were given an intraperitoneal injection of Dyngo-4a (1 mg) or vehicle followed by a booster 4.5–8 h later. BoNT/A (2 LD_{50}) was injected via the tail vein 1.5–2 h following the initial injection. Mice were scored based on their appearance, behavior, and breathing and were euthanized upon reaching acute respiratory distress, indicative of botulism. Mice injected with Dyngo-4a took significantly longer to exhibit clear signs of botulism, 860 ± 65 min compared with 656 ± 55 min. When the data were fitted to a survival curve, a Mantel-Cox test revealed a significant difference ($p = 0.0022$) (Fig. 7*B*) between the two treatments. Mice treated with Dyngo-4a alone or vehicle alone showed no signs of toxicity. Overall, this indicates that Dyngo-4a pretreatment provides significant protection against botulism.

DISCUSSION

In this study we demonstrate that dynamin mediates the activity-dependent uptake of BoNT/A and establish proof of concept that dynamin is a valid pharmacological target for the prevention of botulism. Dynamin is an essential protein implicated in a number of endocytic pathways, including receptor-mediated endocytosis and synaptic vesicle recycling (29, 49). Recently, dynamin was suggested to be involved in the uptake of various other clostridial toxins (28, 45, 46, 50). This can now be confirmed through the use of the recently developed dynamin inhibitors (31, 51–55) such as Dynasore (47) and Dyngo-4a (30). We demonstrate that Dyngo-4a abolished Alexa Fluor 488-BoNT/A-Hc internalization in mature hippocampal neurons and at the amphibian neuromuscular junction at low micromolar concentrations. Overall, our data establish that despite the availability of multiple cellular routes, BoNT/A primarily uses dynamin-dependent processes to enter neurons, mainly via the synaptic vesicle endocytic pathway to block synaptic transmission.

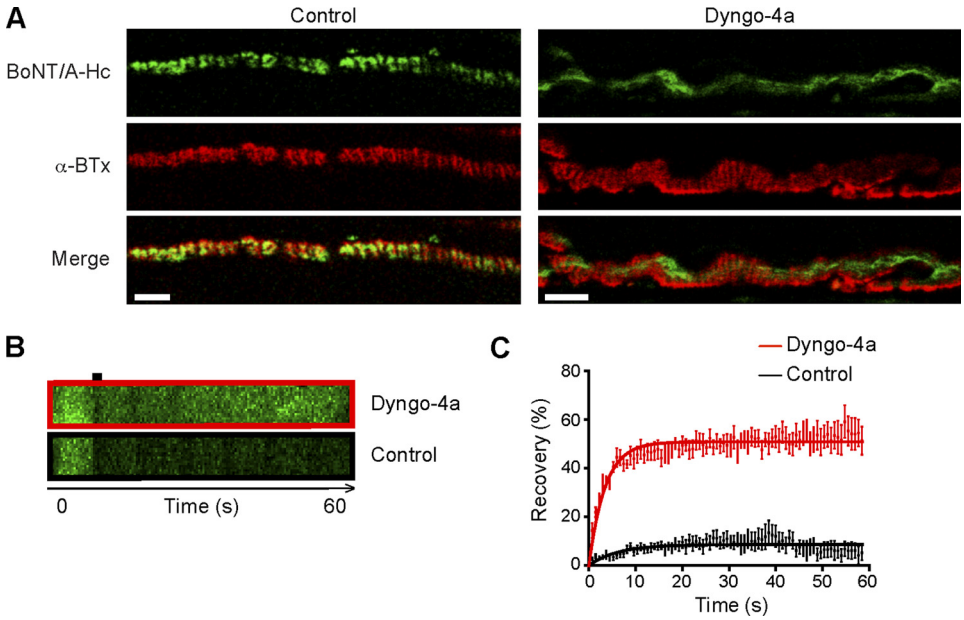

FIGURE 5. *A*, Alexa Fluor 488-BoNT/A-Hc (800 nM) and Alexa Fluor 555-α-bungarotoxin (α-*BTx*, 1 μM) were added to amphibian neuromuscular junction preparations with or without Dyngo-4a (30 μM) in high K^+ frog Ringer's solution for 20 min on ice. Preparations were washed with room temperature normal frog Ringer's solution five times and left in the final wash in the presence or absence of Dyngo-4a. Nerve terminals were visualized with α-bungarotoxin and imaged by confocal microscopy. Representative micrographs are shown. *Scale bars*, 5 μm. *B* and *C*, fluorescence recovery after photobleaching experiments were carried out following a series of 10 images by 20 iterations (100% argon (488 nm) laser power) on identified regions of interest. The recovery was recorded continuously for 1 min thereafter ($n = 3$ terminals per condition). *B*, representative kymographs are also shown. *C*, the recovery of fluorescence intensity immediately after bleaching was graphed. The data were fitted to a one-phase association curve (y = Plateau*(1 − exp (−K*x))), and the mobile and immobile fractions for each condition were determined.

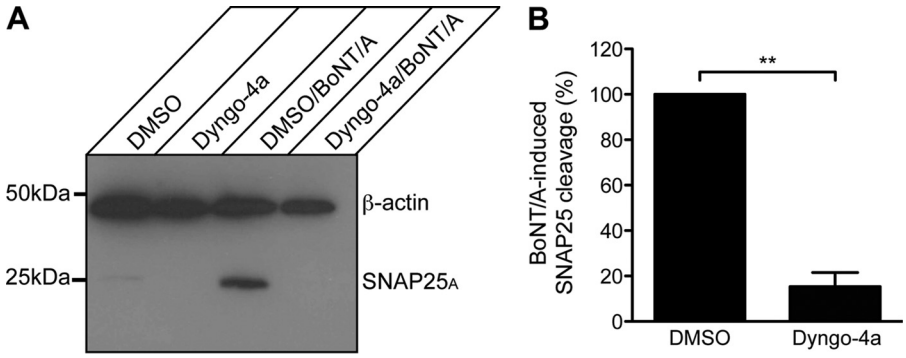

FIGURE 6. **Dyngo-4a prevents SNAP25 cleavage by BoNT/A in cultured hippocampal neurons.** Primary hippocampal neurons were pretreated with Dyngo-4a (30 μM) or DMSO in low K^+ buffer for 20 min before changing the solution to high K^+ buffer containing Dyngo-4a or DMSO in the presence or absence of BoNT/A (100 pM) for 5 min. The cells were washed five times with low K^+ buffer in the continuing presence of Dyngo-4a, incubated for a further 90 min, then transferred to a dish containing an astroglial support culture and conditioned medium for 24 h. *A*, the neurons were processed for Western blotting using an antibody raised against BoNT/A-truncated SNAP25 (37, 38). *B*, the amount of cleaved SNAP25 present in the BoNT/A-treated samples was normalized against β-actin to determine the percentage decrease in the Dyngo-4a-treated samples. A paired *t* test showed a significant reduction in the level of cleaved SNAP25 following treatment with Dyngo-4a (**, $p < 0.01$, ($n = 3$).

The use of Alexa Fluor 488-BoNT/A-Hc to study holotoxin trafficking is warranted by several other studies using recombinant binding domains from various *Clostridium* neurotoxins (18, 28, 56). In good agreement with the recent discovery that BoNT/A binds to the intraluminal domain of the synaptic vesicle protein SV2 (17), we detected a high level of co-localization between Alexa Fluor 488-BoNT/A-Hc and VAMP2 in hippocampal neurons. We found very little overlap between Alexa Fluor 488-BoNT/A-Hc and Rab5 labeling in VAMP2-negative compartments. However, there was a significant overlap among Alexa Fluor 488-BoNT/A-Hc, VAMP2, and Rab5, consistent with the presence of Rab5 on synaptic vesicles (40–42). These results are consistent with the idea that synaptic vesicles recycle through an early endosomal-like compartment (39). Although there was no significant change in co-localization levels at the three time points studied (5, 30, and 60 min), an increased overlap between Alexa Fluor 488-BoNT/A-Hc and VAMP2 labeling was often detected at the later time points.

In line with previous studies using radioiodinated BoNT/A to label murine motor nerve terminals (27, 57, 58), gold-tagged BoNT/A-Hc bound predominantly to the membrane of hippocampal neurons at the level of nerve terminals and was internalized in response to stimulation. In the presynaptic nerve terminals, BoNT/A-Hc was detected predominantly in the lumen of synaptic vesicles, with a smaller proportion present in clathrin-coated structures and early endosomes. BoNT/A-Hc could only be detected in MVBs following a prolonged chase period. MVBs are generated from early endosomes, as the cargo

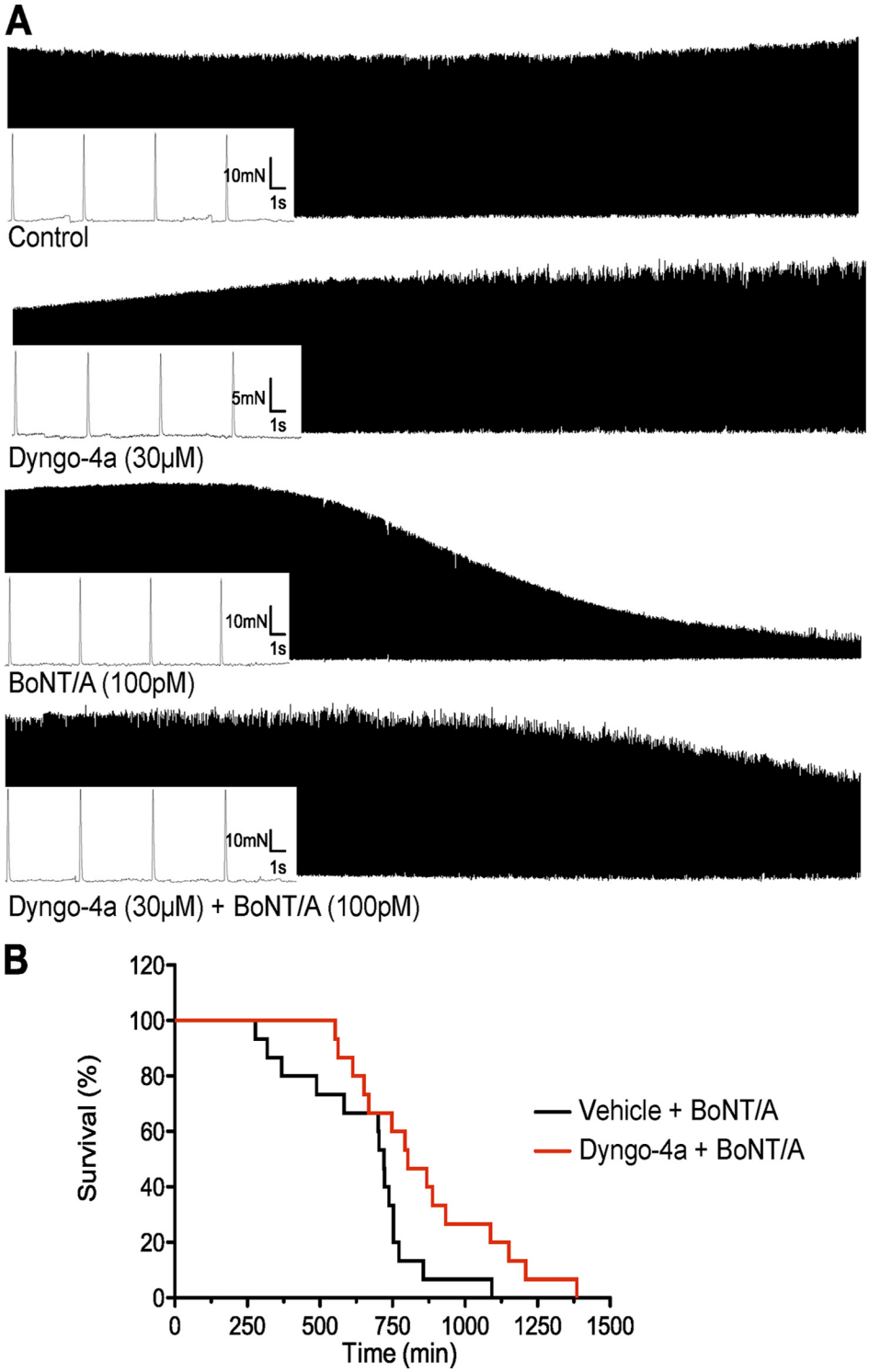

FIGURE 7. **Dyngo-4a provides protection again BoNT/A-induced paralysis in the phrenic nerve-hemidiaphragm twitch model and *in vivo*.** *A*, rat phrenic nerve-hemidiaphragm preparations were stimulated with square pulses of 0.1 ms, 0.2 Hz, 10 V over 6–8 h. Muscles were treated as indicated with Dyngo-4a added 1 h prior to the addition of BoNT/A ($n = 3–9$). The contractile force was measured using a force transducer and recorded through Chart software. Representative traces are shown. *B*, female CD-1 mice (30–40 g) were injected intraperitoneally with Dyngo-4a (1 mg) or vehicle. 1.5–2 h following this injection they were challenged with BoNT/A (2 LD_{50}) injected via the tail vein. A second injection of Dyngo-4a was administered after the first. Several mice were also injected with Dyngo-4a alone or vehicle to ensure that no adverse reactions were produced by these compounds. Mice were monitored for obvious signs of botulism and euthanized when exhibiting clear signs of breathing difficulties. This time was recorded and graphed in a survival time line. A Mantel-Cox test showed that the two curves were significantly different ($n = 10$, *, $p < 0.05$).

proteins destined for degradation partition into intraluminal vesicles formed by invagination of the endosomal vacuole membrane, whereas proteins destined to be recycled are sorted via tubular structures (43, 59). Mature MVBs eventually fuse with lysosomes. The concentration of BoNT/A-Hc on the intraluminal vesicles of MVBs suggests that the toxin is tar-

TABLE 2

Dyngo-4a delays the onset of BoNT/A-induced paralysis in the phrenic nerve-hemidiaphragm twitch preparation

Because each muscle contracts with a different strength, the data from the Dyngo-4a-treated and untreated BoNT/A muscles were normalized and expressed as a percentage. The data were then fitted to a four-parameter logistic curve as described under "Experimental Procedures." Statistical analysis of the $t_{1/2}$ and the Hill slope revealed they were significantly different (**, $p < 0.01$). This indicates that Dyngo-4a delays the onset of BoNT/A-induced paralysis and slows the rate of decline.

Treatment	BoNT/A	Dyngo-4a + BoNT/A
Minimum	15.7 ± 2.2	10.6 ± 6.9
Maxium	95.3 ± 1.9	102.9 ± 1.8
$T_{1/2}$	247.4 ± 2.2	302.7 ± 10.0**
Hill slope	5.83 ± 0.43	3.73 ± 0.33**
R^2	0.9994	0.9999
N	6	9

geted for degradation. Interestingly, BoNT/A has been detected previously in myelinated axons (27), and a proportion of the toxin was recently shown to undergo retrograde transport (60). Delineating the contribution of MVB targeting of BoNT/A to both intoxication and retrograde transport/degradation of the toxin-receptor complex will be an important future endeavor.

Our results clearly show that Dyngo-4a as well as Dynasore could prevent the internalization of BoNT/A-Hc. This block was sufficient to prevent SNAP25 cleavage in hippocampal neurons. Importantly, although blockade of exocytosis and SNAP25 cleavage is highly correlated in cultured neurons (61) and neurosecretory cells (62, 63), this is not the case at the motor nerve terminal where only marginal cleavage can result in full paralysis (64). This prompted our investigation at the amphibian neuromuscular junction and rat hemidiaphragm preparation. To our surprise, Dyngo-4a treatment offered significant protection against BoNT/A-induced paralysis. Furthermore, Dyngo-4a significantly delayed the onset of botulism by >30%. To the best of our knowledge, our study is the first to highlight the role of dynamin in BoNT internalization in neurons and motor nerve terminals. More work is required to test the efficacy of higher doses of Dyngo-4a and other dynamin inhibitors and to determine the window of opportunity allowing for therapeutic intervention following exposure to the neurotoxin.

Interestingly, Dyngo-4a did not impact on neurotransmitter release at low levels of stimulation for up to 8 h in a hemidiaphragm twitch experiment. Furthermore, control mice did not appear to be affected by Dyngo-4a treatment, suggesting that dampening dynamin function does not preclude normal physiological function. This may be due to the low level of stimulation used in our study. It is likely, however, that at higher frequencies, neurotransmitter release will not be sustainable in the presence of dynamin inhibitors as recently demonstrated (65–67). Longer treatment and increased stimulation regimes are therefore warranted to determine the safety margin of treatments based on the use of dynamin inhibitors.

Currently, antitoxins and vaccines are the only available therapies against botulism. Because these treatments are not readily available to the public (7), more cost-effective and efficacious antibodies are continually being sought (68). Inhibitors capable of delaying the onset of botulism by blocking BoNT-Lc activity have also been described (8, 69). Although these compounds generally work better *in vitro* (69, 70), some have led to 60% of treated mice surviving 3-fold longer than controls (8). One pitfall of these molecules is that they are only effective against a specific serotype. One of the best BoNT/A inhibitors found to date is toosendanin, shown to lead to a 4-fold increase in survival time by interfering with the translocation process (71) rather than cellular entry mechanisms.

Our study establishes the internalization step as a valid target for preventing BoNT-induced paralysis, and our data highlight the therapeutic potential of this trafficking strategy. As all serotypes of BoNT are likely to take advantage of a similar internalization mechanism, dynamin inhibition may well be efficient for all serotypes, although this needs to be investigated. Our results suggest that dynamin inhibitors could also prolong the therapeutic window available for the use of antitoxins by delaying the neuronal uptake of BoNTs and providing extra time for the antibodies to be effective.

In summary, our data reveal that BoNT internalization in nerve terminals is primarily dynamin-dependent and utilizes synaptic vesicle endocytosis and the endosomal pathways. This specificity can be capitalized upon to prevent toxin uptake by the use of dynamin inhibitors. Although more work is required to design dynamin inhibitors with increased potency against BoNT internalization, our study establishes dynamin as a valid drug target for the design of further small molecules for the prevention of botulism.

Acknowledgments—Electron microscopy was performed in the Australian Microscopy and Microanalysis Facility (AMMRF) at the Centre for Microscopy and Microanalysis at the University of Queensland and the in vivo experiments at the University of Queensland (Princess Alexandra Hospital) Breeding and Research Facilities. We thank Cliff Shone (Health Protection Agency, United Kingdom) for providing botulinum neurotoxin type A and Rowan Tweedale and Shona Osborne for critical comments.

REFERENCES

1. Meunier, F. A., Colasante, C., and Molgo, J. (1997) *Neuroscience* **78,** 883–893
2. Meunier, F. A., Mattei, C., Chameau, P., Lawrence, G., Colasante, C., Kreger, A. S., Dolly, J. O., and Molgó, J. (2000) *J. Cell Sci.* **113,** 1119–1125
3. Meunier, F. A., Feng, Z. P., Molgó, J., Zamponi, G. W., and Schiavo, G. (2002) *EMBO J.* **21,** 6733–6743
4. Arnon, S. S., Schechter, R., Inglesby, T. V., Henderson, D. A., Bartlett, J. G., Ascher, M. S., Eitzen, E., Fine, A. D., Hauer, J., Layton, M., Lillibridge, S., Osterholm, M. T., O'Toole, T., Parker, G., Perl, T. M., Russell, P. K., Swerdlow, D. L., and Tonat, K. (2001) *JAMA* **285,** 1059–1070
5. Osborne, S. L., Latham, C. F., Wen, P. J., Cavaignac, S., Fanning, J., Foran, P. G., and Meunier, F. A. (2007) *J. Neurosci. Res.* **85,** 1149–1158
6. Foran, P. G., Davletov, B., and Meunier, F. A. (2003) *Trends Mol. Med.* **9,** 291–299
7. Rusnak, J. M., and Smith, L. A. (2009) *Hum. Vaccin.* **5,** 794–805
8. Pang, Y. P., Davis, J., Wang, S., Park, J. G., Nambiar, M. P., Schmidt, J. J., and Millard, C. B. (2010) *PLoS One* **5,** e10129
9. Schiavo, G., Matteoli, M., and Montecucco, C. (2000) *Physiol. Rev.* **80,** 717–766
10. de Paiva, A., Meunier, F. A., Molgó, J., Aoki, K. R., and Dolly, J. O. (1999) *Proc. Natl. Acad. Sci. U.S.A.* **96,** 3200–3205
11. Lacy, D. B., Tepp, W., Cohen, A. C., DasGupta, B. R., and Stevens, R. C. (1998) *Nat. Struct. Biol.* **5,** 898–902
12. Simpson, L. L., and Rapport, M. M. (1971) *J. Neurochem.* **18,** 1751–1759
13. Montecucco, C. (1986) *Trends Biochem. Sci.* **11,** 314–317

14. Nishiki, T., Kamata, Y., Nemoto, Y., Omori, A., Ito, T., Takahashi, M., and Kozaki, S. (1994) *J. Biol. Chem.* **269,** 10498–10503
15. Rummel, A., Eichner, T., Weil, T., Karnath, T., Gutcaits, A., Mahrhold, S., Sandhoff, K., Proia, R. L., Acharya, K. R., Bigalke, H., and Binz, T. (2007) *Proc. Natl. Acad. Sci. U.S.A.* **104,** 359–364
16. Rummel, A., Karnath, T., Henke, T., Bigalke, H., and Binz, T. (2004) *J. Biol. Chem.* **279,** 30865–30870
17. Dong, M., Yeh, F., Tepp, W. H., Dean, C., Johnson, E. A., Janz, R., and Chapman, E. R. (2006) *Science* **312,** 592–596
18. Fu, Z., Chen, C., Barbieri, J. T., Kim, J. J., and Baldwin, M. R. (2009) *Biochemistry* **48,** 5631–5641
19. Koriazova, L. K., and Montal, M. (2003) *Nat. Struct. Biol.* **10,** 13–18
20. Schiavo, G., Shone, C. C., Rossetto, O., Alexander, F. C., and Montecucco, C. (1993) *J. Biol. Chem.* **268,** 11516–11519
21. Schiavo, G., Rossetto, O., Catsicas, S., Polverino de Laureto, P., DasGupta, B. R., Benfenati, F., and Montecucco, C. (1993) *J. Biol. Chem.* **268,** 23784–23787
22. Foran, P., Lawrence, G. W., Shone, C. C., Foster, K. A., and Dolly, J. O. (1996) *Biochemistry* **35,** 2630–2636
23. Blasi, J., Chapman, E. R., Link, E., Binz, T., Yamasaki, S., De Camilli, P., Südhof, T. C., Niemann, H., and Jahn, R. (1993) *Nature* **365,** 160–163
24. Chen, S., and Barbieri, J. T. (2011) *J. Biol. Chem.* **286,** 15067–15072
25. Schiavo, G., Santucci, A., Dasgupta, B. R., Mehta, P. P., Jontes, J., Benfenati, F., Wilson, M. C., and Montecucco, C. (1993) *FEBS Lett.* **335,** 99–103
26. Darios, F., Niranjan, D., Ferrari, E., Zhang, F., Soloviev, M., Rummel, A., Bigalke, H., Suckling, J., Ushkaryov, Y., Naumenko, N., Shakirzyanova, A., Giniatullin, R., Maywood, E., Hastings, M., Binz, T., and Davletov, B. (2010) *Proc. Natl. Acad. Sci. U.S.A.* **107,** 18197–18201
27. Black, J. D., and Dolly, J. O. (1986) *J. Cell Biol.* **103,** 521–534
28. Couesnon, A., Shimizu, T., and Popoff, M. R. (2009) *Cell Microbiol.* **11,** 289–308
29. Praefcke, G. J., and McMahon, H. T. (2004) *Nat. Rev. Mol. Cell Biol.* **5,** 133–147
30. Howes, M. T., Kirkham, M., Riches, J., Cortese, K., Walser, P. J., Simpson, F., Hill, M. M., Jones, A., Lundmark, R., Lindsay, M. R., Hernandez-Deviez, D. J., Hadzic, G., McCluskey, A., Bashir, R., Liu, L., Pilch, P., McMahon, H., Robinson, P. J., Hancock, J. F., Mayor, S., and Parton, R. G. (2010) *J. Cell Biol.* **190,** 675–691
31. Hill, T. A., Gordon, C. P., McGeachie, A. B., Venn-Brown, B., Odell, L. R., Chau, N., Quan, A., Mariana, A., Sakoff, J. A., Chircop, M., Robinson, P. J., and McCluskey, A. (2009) *J. Med. Chem.* **52,** 3762–3773
32. Kaech, S., and Banker, G. (2006) *Nat. Protoc.* **1,** 2406–2415
33. Wen, P. J., Osborne, S. L., Morrow, I. C., Parton, R. G., Domin, J., and Meunier, F. A. (2008) *Mol. Biol. Cell* **19,** 5593–5603
34. Slot, J. W., and Geuze, H. J. (1985) *Eur. J. Cell Biol.* **38,** 87–93
35. Slot, J. W., and Geuze, H. J. (1981) *J. Cell Biol.* **90,** 533–536
36. Meunier, F. A., Nguyen, T. H., Colasante, C., Luo, F., Sullivan, R. K., Lavidis, N. A., Molgó, J., Meriney, S. D., and Schiavo, G. (2010) *J. Cell Sci.* **123,** 1131–1140
37. Meunier, F. A., Lisk, G., Sesardic, D., and Dolly, J. O. (2003) *Mol. Cell. Neurosci.* **22,** 454–466
38. Ekong, T. A., Feavers, I. M., and Sesardic, D. (1997) *Microbiology* **143,** 3337–3347
39. de Hoop, M. J., Huber, L. A., Stenmark, H., Williamson, E., Zerial, M., Parton, R. G., and Dotti, C. G. (1994) *Neuron* **13,** 11–22
40. Fischer von Mollard, G., Stahl, B., Walch-Solimena, C., Takei, K., Daniels, L., Khoklatchev, A., De Camilli, P., Südhof, T. C., and Jahn, R. (1994) *Eur. J. Cell Biol.* **65,** 319–326
41. Wucherpfennig, T., Wilsch-Bräuninger, M., and González-Gaitán, M. (2003) *J. Cell Biol.* **161,** 609–624
42. Takamori, S., Holt, M., Stenius, K., Lemke, E. A., Grønborg, M., Riedel, D., Urlaub, H., Schenck, S., Brügger, B., Ringler, P., Müller, S. A., Rammner, B., Gräter, F., Hub, J. S., De Groot, B. L., Mieskes, G., Moriyama, Y., Klingauf, J., Grubmüller, H., Heuser, J., Wieland, F., and Jahn, R. (2006) *Cell* **127,** 831–846
43. Piper, R. C., and Luzio, J. P. (2001) *Traffic* **2,** 612–621
44. Yeh, F. L., Dong, M., Yao, J., Tepp, W. H., Lin, G., Johnson, E. A., and Chapman, E. R. (2010) *PLoS Pathog.* **6,** e1001207
45. Deinhardt, K., Berninghausen, O., Willison, H. J., Hopkins, C. R., and Schiavo, G. (2006) *J. Cell Biol.* **174,** 459–471
46. Pust, S., Barth, H., and Sandvig, K. (2010) *Cell. Microbiol.* **12,** 1809–1820
47. Macia, E., Ehrlich, M., Massol, R., Boucrot, E., Brunner, C., and Kirchhausen, T. (2006) *Dev. Cell* **10,** 839–850
48. Simpson, L. L. (1973) *Neuropharmacology* **12,** 165–176
49. Hayashi, M., Raimondi, A., O'Toole, E., Paradise, S., Collesi, C., Cremona, O., Ferguson, S. M., and De Camilli, P. (2008) *Proc. Natl. Acad. Sci. U.S.A.* **105,** 2175–2180
50. Gibert, M., Monier, M. N., Ruez, R., Hale, M. L., Stiles, B. G., Benmerah, A., Johannes, L., Lamaze, C., and Popoff, M. R. (2011) *Cell. Microbiol.* **13,** 154–170
51. Hill, T., Odell, L. R., Edwards, J. K., Graham, M. E., McGeachie, A. B., Rusak, J., Quan, A., Abagyan, R., Scott, J. L., Robinson, P. J., and McCluskey, A. (2005) *J. Med. Chem.* **48,** 7781–7788
52. Hill, T. A., Mariana, A., Gordon, C. P., Odell, L. R., Robertson, M. J., McGeachie, A. B., Chau, N., Daniel, J. A., Gorgani, N. N., Robinson, P. J., and McCluskey, A. (2010) *J. Med. Chem.* **53,** 4094–4102
53. Hill, T. A., Odell, L. R., Quan, A., Abagyan, R., Ferguson, G., Robinson, P. J., and McCluskey, A. (2004) *Bioorg. Med. Chem. Lett.* **14,** 3275–3278
54. Newton, A. J., Kirchhausen, T., and Murthy, V. N. (2006) *Proc. Natl. Acad. Sci. U.S.A.* **103,** 17955–17960
55. Odell, L. R., Howan, D., Gordon, C. P., Robertson, M. J., Chau, N., Mariana, A., Whiting, A. E., Abagyan, R., Daniel, J. A., Gorgani, N. N., Robinson, P. J., and McCluskey, A. (2010) *J. Med. Chem.* **53,** 5267–5280
56. Lalli, G., Herreros, J., Osborne, S. L., Montecucco, C., Rossetto, O., and Schiavo, G. (1999) *J. Cell Sci.* **112,** 2715–2724
57. Black, J. D., and Dolly, J. O. (1986) *J. Cell Biol.* **103,** 535–544
58. Dolly, J. O., Black, J., Williams, R. S., and Melling, J. (1984) *Nature* **307,** 457–460
59. Woodman, P. G., and Futter, C. E. (2008) *Curr. Opin. Cell Biol.* **20,** 408–414
60. Antonucci, F., Rossi, C., Gianfranceschi, L., Rossetto, O., and Caleo, M. (2008) *J. Neurosci.* **28,** 3689–3696
61. Foran, P. G., Mohammed, N., Lisk, G. O., Nagwaney, S., Lawrence, G. W., Johnson, E., Smith, L., Aoki, K. R., and Dolly, J. O. (2003) *J. Biol. Chem.* **278,** 1363–1371
62. Lawrence, G. W., Foran, P., and Dolly, J. O. (1996) *Eur. J. Biochem.* **236,** 877–886
63. Lawrence, G. W., Weller, U., and Dolly, J. O. (1994) *Eur. J. Biochem.* **222,** 325–333
64. Raciborska, D. A., and Charlton, M. P. (1999) *Can. J. Physiol. Pharmacol.* **77,** 679–688
65. Chung, C., Barylko, B., Leitz, J., Liu, X., and Kavalali, E. T. (2010) *J. Neurosci.* **30,** 1363–1376
66. Douthitt, H. L., Luo, F., McCann, S. D., and Meriney, S. D. (2011) *Neuroscience* **172,** 187–195
67. Clayton, E. L., Anggono, V., Smillie, K. J., Chau, N., Robinson, P. J., and Cousin, M. A. (2009) *J. Neurosci.* **29,** 7706–7717
68. Cheng, L. W., Stanker, L. H., Henderson, T. D., 2nd, Lou, J., and Marks, J. D. (2009) *Infect. Immun.* **77,** 4305–4313
69. Eubanks, L. M., Hixon, M. S., Jin, W., Hong, S., Clancy, C. M., Tepp, W. H., Baldwin, M. R., Malizio, C. J., Goodnough, M. C., Barbieri, J. T., Johnson, E. A., Boger, D. L., Dickerson, T. J., and Janda, K. D. (2007) *Proc. Natl. Acad. Sci. U.S.A.* **104,** 2602–2607
70. Roxas-Duncan, V., Enyedy, I., Montgomery, V. A., Eccard, V. S., Carrington, M. A., Lai, H., Gul, N., Yang, D. C., and Smith, L. A. (2009) *Antimicrob. Agents Chemother.* **53,** 3478–3486
71. Fischer, A., Nakai, Y., Eubanks, L. M., Clancy, C. M., Tepp, W. H., Pellett, S., Dickerson, T. J., Johnson, E. A., Janda, K. D., and Montal, M. (2009) *Proc. Natl. Acad. Sci. U.S.A.* **106,** 1330–1335